Contrast Enhancement in Wavelet Domain for Graph-based Segmentation in Medical Imaging

Sarada Prasad Dakua* and Julien Abi-Nahed
Qatar Science & Technology Park/Qatar Robotic Surgery Center
Qatar Foundation, Education city, Doha
P.O. Box 210000, Qatar
sdakua@qstp.org.qa, jabinahed@qstp.org.qa

ABSTRACT

Despite increased image quality including medical imaging, image segmentation continues to represent a major bottleneck in practical applications due to noise and lack of contrast. In this paper, we present a new methodology to segment low contrast medical images. There are two stages to this approach, 1) a contrast enhancement stage, that uses stochastic resonance theory applied in a wavelet domain, is performed by utilizing the noise present in medical data, and 2) a new weighting function is proposed for traditional graph-based approaches. Both qualitative and quantitative evaluation performed on publicly available databases of two imaging modalities reflect the potential of the proposed method.

Keywords

CT, MR, image segmentation, liver, heart.

1. INTRODUCTION

The study of the shape and motion of heart or liver is important because many heart or liver diseases are thought to be strongly correlated to the shape and motion of the heart or liver and the segmentation provides adequate information about the shape and size of an object; some prominent examples of such heart diseases include ischemia and right ventricle (RV) hypertrophy. If we consider manual segmentation, it is not only a tedious and time consuming process but also an inaccurate one, it is therefore desirable to use algorithms that are accurate and require little user interaction. Cardiac magnetic resonance (CMR) imaging is a leading modality for imaging the heart and clinical diagnosis, due to some of its remarkable advantages [1]. Segmentation of left ventricle (LV) in CMR images, obtained from a patient having serious ischemia, is difficult. In this type of images, LV is nearly indistinguishable from the surrounding muscles to the naked eye. Such ischemic CMR (obscure) images are the input in this experiment. In order to get significant information regarding LV, contour of blood pool and left ventricular myocardial wall need to be drawn, 1) inner contour (endocardial wall or blood pool boundary) and 2) outer contour (epicardial wall). The outer contour is comparatively difficult to extract due to small variation in intensity in this region. A rich tradition of work in image segmentation has focused on the establishment of appropriate image (object) models. A state of the art on recent segmentation algorithms has been presented in [2]. Because of the space constraint, we restrict ourselves to only a few of them. Although level set methods gained tremendous popularity, still some problems like computational complexity, re-initialization [3, 4] of the zero level set exist. In the early level set methods, the computation is carried out on the entire domain making the computation slow. Narrow band level set methods [5] restrict the computation to a narrow band around the zero level set, but it does not reduce the computational cost to a reasonable limit [6]. Active contours without edges [7] is useful in detecting the object edge irrespective of the initial contour placement. At the same time, mean intensities of all the regions must be different for a successful segmentation. Atlas-guided approaches have been applied mainly in MR brain imaging. An advantage of atlas-guided approaches is that labels are transferred as well as the segmentation. They also provide a standard system for studying morphometric properties [8]. Even with non-linear registration methods, however, accurate segmentations of complex structures is difficult due to anatomical variability. Moreover, atlas-based segmentation has been of limited use in presence of large space-occupying lesions [9]. The watershed algorithm uses concepts from mathematical morphology to partition images into homogeneous regions [10]. This method can suffer from over-segmentation, which occurs when the image is segmented into an unnecessarily large number of regions. Thus, watershed algorithms in medical imaging are usually followed by a postprocessing step to merge separate regions that belong to the same structure [11]. There are also many model based segmentation techniques [1]. One substantial limitation of such methods is that their accuracy may be restricted either by the uncertainties in image content or by the intrinsic properties by the model itself, such as prior shape constraints [12] and the list of methods goes on. A fast and semi-automatic algorithm proposed in [15] comes under this category and is based on Random Walk. It does not suffer from the "small cut" problem and extends naturally to an arbitrary number of labels;

*Corresponding author

ICVGIP '12, December 16-19, 2012, Mumbai, India

we incline more towards this method due to various other advantages such as 1) noise robustness, 2) usage of only one free parameter, and 3) fast computation and editing. The concept of Random Walk originates from the physical and mathematical model of Brownian motion. It is the formalization of the intuitive idea of taking successive steps in random directions, like a molecule traveling in a liquid or gas. L. Grady successfully transferred this idea to the field of image segmentation. For this purpose he transforms the image into an undirected weighted graph $G = (Nodes, Edges)$. So the Random Walk segmentation is based on graph theory. Seed points are used to indicate different objects and the method returns a probability map for each seeded region.

Over the years, several methods have been proposed to tackle the segmentation problem in noisy and cluttered medical images. Typical use of filtering (as reported by these methods) leads to degradation in the image quality, therefore in our approach, we utilize the noise in a constructive manner. One of the efficient approaches that utilizes noise to enhance the contrast of a low contrast input image is stochastic resonance (SR). Apart from a few attempts e.g. [13], SR is yet to gain the full attention of the image processing community. In this paper, we have applied SR to image enhancement, followed by a new weighting function for graph-based approach for image segmentation.

1.1 Image Enhancement using SR

Image enhancement is the process of improving the quality of the digital image without knowledge about the source of degradation. In this work, our aim is to enhance low contrast images, without introducing any blocking artifacts, by using SR phenomenon. The effect requires three basic ingredients: (i) an energetic activation barrier or, more generally, a form of threshold; (ii) a weak coherent input (such as a periodic signal); (iii) a source of noise that is inherent in the system, or that adds to the coherent input. Given these features, the response of the system undergoes resonance-like behavior as a function of the noise level; hence the name stochastic resonance. SR occurs if the signal-to-noise ratio (SNR) and input/output correlation have a well-marked maximum at a certain noise level [13]. Unlike very low or high noise intensities, moderate ones allow the signal to cross the threshold, giving maximum SNR at some optimum noise level. In the bistable SR model (Figure 1 (a) of [13]), upon addition of zero mean Gaussian noise, the pixel is transferred from a weak signal state to a strong signal state, described by Brownian motion of a particle placed in a double well potential system. In the context of this paper, the double well represents the contrast of an image and the position of the particle as the intensity values. The state, at which performance metrics [13] are found optimum, can be considered as the stable state that provides maximum SNR. On increasing the number of iterations beyond this, the state becomes oscillatory. Some researchers have attempted to use SR in Fourier or spatial domains [13], however we have chosen the wavelet transform domain as explained in the next section.

2. MATERIALS AND METHODS

Our proposed methodology is divided into two modules: image enhancement with SR, and graph-based segmentation applied to the contrast enhanced image using the new proposed weighting function. Due to page constraints, this section explains each module briefly. One of the commonly used techniques for image resolution enhancement is Interpolation. Interpolation has been widely used in many image processing applications such as facial reconstruction, multiple description coding, and super resolution. There are three well known interpolation techniques, namely nearest neighbor interpolation, bilinear interpolation, and bi-cubic interpolation. The main disadvantage in using interpolation the loss of HF components (Edges), which is due to the smoothing caused by interpolation. Preserving the edges is essential; to avoid this problem we use the tool called wavelet transform because the discrete wavelet transform (DWT) domain provides the space-frequency localization and this characteristic enables one to enhance features by treating the sub-bands at different scales, leading to a high quality of enhancement.

2.1 Discrete Mathematics for Proposed DWT-based SR

The DWT is used to divide the image into sub-bands. We know that the edges are concentrated on LH, HL, HH sunbands. Hence even if we separate the HF components and apply some transformations on the LF will not cause any damage to the edge components. Hence after reconstruction the image looks sharper too. In this methodology, 2-D discrete wavelet transform is applied to the $M \times N$ size image I. Applying SR to the approximation and detail coefficients, the stochastically enhanced (tuned) coefficient-sets in DWT domain are obtained as $W_{\psi}^{s}(l,p,q)_{DSR}$ and $W(l_0,p,q)_{DSR}$. The SR in discrete form is defined as:

$$\frac{dx}{dt} = \left[ax - bx^3\right] + B\sin\omega t + \sqrt{D}\xi(t) \tag{1}$$

where $\sqrt{D}\xi(t)$ and $B\sin\omega t$ represent noise and input, respectively; these are replaced by DWT sub-band coefficients. The noise term is the cause in producing SR; the maximization of SNR occurs at the double well parameter a. The (1) is solved (as in [14]) before the actual SR implementation on digital images. The low contrast image may be viewed as a noisy image containing internal noise due to lack of illumination. This noise is inherent in its DWT coefficients and therefore, the DWT coefficients can be viewed as containing signal (image information) as well as noise. The final stochastic simulation is obtained after some predefined number of iterations. Given the tuned (enhanced and stabilized) set of wavelet coefficients ($X_{\phi}(l_0,p,q)$ and $X_{\psi}^{s}(l,p,q)$), the enhanced image $I_{enhanced}$ in spatial domain is obtained by inverse discrete wavelet transform (IDWT) given as:

$$\begin{aligned} I_{enhanced} = {} & \frac{1}{\sqrt{MN}} \sum_{p}\sum_{q} X_{\phi}(l_0,p,q)\,\phi_{l_0,p,q}(i,j) + \\ & \frac{1}{\sqrt{MN}} \sum_{s\in(H,V,D)} \sum_{l=l_0} \sum_{p}\sum_{q} X_{\psi}^{s}(l,p,q)\,\psi_{l_0,p,q}^{s}(i,j) \end{aligned} \tag{2}$$

This is the enhanced image after n iterations. The determination of double well parameters a and b (from the SNR) is omitted from the discussion due to page constraints.

2.2 Enhancement Algorithm

The method can be briefly described as: 1) the input image is decomposed through DWT, 2) assuming an initial value for the bistable parameters, the intensity values (gray levels) are tuned using SR (following an iterative/sequential procedure), and 3) the parameters are optimized with respect to the performance metrics [13] such as, Metric of Con-

trast Enhancement and Perceptual Quality Metric. After image enhancement, a graph-based method, such as Random Walk, is adopted to segment the image.

2.3 Random Walk-based Segmentation

The Random Walk segmentation is based on graph theory (readers may refer [15] for extensive details). Random walk (RW), or drunkards walk, was one of the first chance-processes studied in the theory of probability and has gained a lot of attention in several areas in visual computing. The name random walk is used because one may think of it as being a model for an individual walking on a straight line who at each point of time either takes one step to the right with probability p or one step to the left with probability $1-p$, for example. Given a graph and a starting node, one selects one of its neighbor at random and moves to this neighbor then selects a neighbor of this node at random and moves to it and so on. This sequence of nodes selected randomly this way is a random walk on the graph. The segmentation method to be proposed applies random walks on a graph whose nodes are the input points, and whose links represents the connectivity between them. When applied on an image, initially, seeds are required to be placed on different labels (homogeneous regions to be segmented) so that at least one seed must be defined for each region. If there are K number of seeds, there will a K-tuple probability vector for each pixel, given a random walker starting at this location. A final segmentation is derived from these K-tuples by selecting for each pixel the most probable seed destination for the random walker.

Influence of Weighting Function :

In the process of segmentation using Random Walk, the weighting function is used to map a change in image intensities to edge weights. The performance of any graph-based segmentation depends on the choice of this weighting function [16]. The performance of Gaussian weighting function is perfect in clean images [15]. However on cardiac magnetic resonance (CMR) images, the level of performance decreases significantly (as shown in Results and Conclusions section). In this work, we suggest a new weighting function that improves the performance of Laplacian operator at the fundamental level.

2.4 Derivative of Laplacian of Gaussian Weighting Function

A blurred edge $v(x)$ can be represented by a combination of an exponential and a step function:

$$v(x) = \begin{cases} e^{\left(-\frac{(x-t)^2}{2\sigma_s^2}\right)}, & x \leq t \\ 1, & x > t, \end{cases} \tag{3}$$

where t represents the width of the region of interest (ROI) and σ_s the extent of the blurring, $(0 \leqslant \sigma_s \leqslant S,\ S \in \mathbb{R})$, $\sigma_s = \begin{cases} S, & \text{blurred edge} \\ 0, & \text{sharp edge} \end{cases}$. The quantity of blurring increases with increase in S. If E_c is the characteristic function of matching of an input object with the output (i.e., matching of two ROIs; due to edge and weighting function), then ${E_c}_v^w$ (characteristic function with respect to an edge, v, and a weighting function, w) determines if a feature is worth tracking for segmentation. In other words, the characteristic function determines the suitability of a weighting function to a particular edge for its detection.

Characteristic function : In the continuous setting, a weight is a positive measure such as $w(x)\,dx$ on some domain, which is typically a subset of a Euclidean space (presently, rather we consider pixel intensity). In this context, the weight function $w(x)$ is sometimes referred to as a density. Conceptually, the characteristic function ${E_c}_v^w$ is defined as:

$${E_c}_v^w = \int_0^{2t} v(x)\, w(x)\, dx. \tag{4}$$

If the right hand side of (4) is more, then the edge characteristic will be more dense in regard to blurring. Therefore, it must be desirable to have a lower magnitude of ${E_c}_v^w$. The derivative of Laplacian of Gaussian (DroLoG) weighting function is defined as

$$w_{DroLoG} = \frac{x^2 - 2\sigma_1^2}{\sigma_1^4} e^{-\frac{x^2}{2\sigma_1^2}} - \frac{x^2 - 2\sigma_2^2}{\sigma_2^4} e^{-\frac{x^2}{2\sigma_2^2}} \tag{5}$$

where σ and w_{LoG} are usual standard deviation and Laplacian of Gaussian weighting function, respectively. Let the error function due to Gaussian weighting function be

$$E_v^G = \int_0^{2t} v(x)\, w_{Gauss}(x)\, dx. \tag{6}$$

and similarly for DroLoG.The difference between two characteristic functions is expressed as

$$\hbar = E_v^{DroLoG} - E_v^G \tag{7}$$

where :

$$\begin{aligned} \hbar \;=\; & \sqrt{\frac{1}{2\pi}}\frac{1}{\sigma^7}\left[e^{\left(1+\frac{3t(\ln t-1)-\left(\frac{1}{\sigma_s^2}+\frac{1}{\sigma^2}\right)\left(\frac{t^3}{6}\right)+\frac{t^2}{4\sigma_s^2}}{t^3 e^{-\left(\frac{1}{\sigma_s^2}+\frac{1}{\sigma^2}\right)\frac{t^2}{2}}}\right)} - \frac{1}{2}\left(\frac{1}{2\sigma^2}\right)^{-2} \right. \\ & \left. \left(\Gamma\left(2, \frac{2t^2}{\sigma^2}\right) - \Gamma\left(2, \frac{t^2}{2\sigma^2}\right)\right)\right] - \sqrt{\frac{1}{2\pi}}\frac{1}{\sigma}\left[\sqrt{\frac{\pi}{8}}\right. \\ & \frac{1}{\left(\frac{1}{\sigma_s^2}+\frac{1}{\sigma^2}\right)^{\frac{3}{2}}}\left(\left(\frac{t}{\sigma_s^2}\right)^2 - \left(\frac{1}{\sigma_s^2}+\frac{1}{\sigma^2}\right)\left(\frac{t^2}{\sigma_s^2}\right)\right) \\ & \left\{ erf\left(\left(\sqrt{\frac{1}{2\sigma_s^2}+\frac{1}{2\sigma^2}}t\right) - \frac{\frac{2t}{\sigma_s^2}}{\sqrt{\left(\frac{1}{\sigma_s^2}+\frac{1}{\sigma^2}\right)}}\right) - \right. \\ & \left. erf\left(\frac{-\frac{2t}{\sigma_s^2}}{\sqrt{\left(\frac{1}{\sigma_s^2}+\frac{1}{\sigma^2}\right)}}\right)\right\} + 2\sigma\sqrt{\pi}\left\{ erf\left(\frac{\sqrt{2}t}{\sigma}\right) - \right. \\ & \left. \left. erf\left(\frac{t}{\sqrt{2}\sigma}\right)\right\}\right] \end{aligned} \tag{8}$$

where erf is the error function and $\Gamma(a,x) = \int_z^\infty e^{-t} t^{a-1} dt$. A graphical analysis of $E_v^{DroLoG} - E_v^G$ is possible by varying values of t, σ individually. In order to show the effect of blurring on the above difference, only σ_s is varied. Though

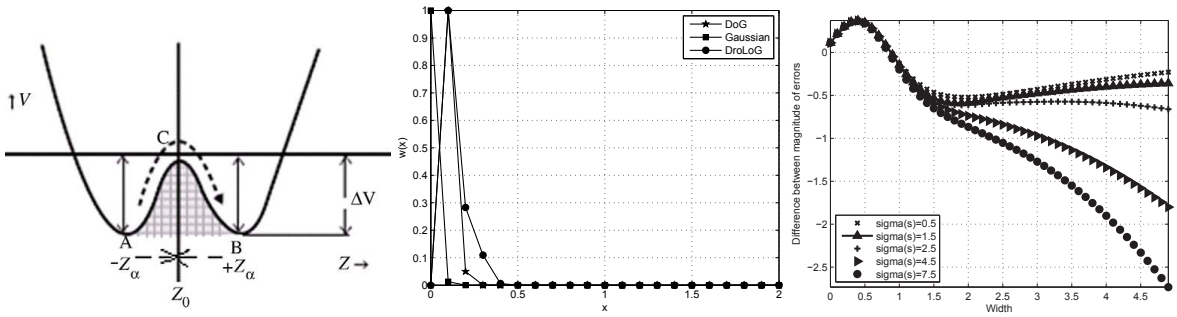

(a) (b) (c)

Figure 1: (a) SR in biphasic form: The dashed arrow represents the transition under noise, crossing over the shaded threshold C [13]. (b) Weighting functions. (c) Difference of characteristic functions.

for small values of edge variance σ_s (steeper edge), the plot shows negative values of $E_v^{DroLoG} - E_v^G$ for $t > 1$, simultaneously, it is also observed (Figure 1(c)) that with increase in t, the curves corresponding to low values of σ_s are not monotonically decreasing. As the edge variance increases (i.e. the edge becomes blurred), for example when σ_s =2.5, 4.5, and 7.5, the plot shows increasingly negative values for $(E_v^{DroLoG} - E_v^G)$, which reflects DroLoG as the better option than Gaussian in case of blurry edge images.

3. RESULTS AND CONCLUSIONS

The test liver CT and CMR datasets were obtained from MICCAI 2007 Grand Challenge and [18], respectively. Figure 2 shows the contrast enhancement and segmentation results of the liver CT and CMR images. For CMR images, only the endocardium is obtained by the proposed method. The epicardium is obtained by a modified active contour model [17] that considers endocardium as its initial contour. In order to compare the degree of superiority, the combined segmentation algorithm is implemented using both the weighting functions. It may be observed that papillary muscles get well segmented in case of DroloG. This is because DroLoG has moderate decreasing rate (Figure 1(b)) as compared to Gaussian and Difference of Gaussian (DoG), DroLoG achieves necessary characteristics to produce a better segmentation. The computational cost per iteration is linear in the number of pixels. The required number of iterations depends greatly on the time step dt and the initialization. The average number of iterations is 50. It takes nearly 4 to 6 sec to perform segmentation by a 2GB RAM and core2duo processor on a single CMR image. The employed metrics for quantitative evaluation are provided in Table 1 that includes Hausdorff's distance (H_d), precision, accuracy, and mean error rate (MER). On MICCAI dataset (45 subjects), as reference, one of the best methods of MICCAI 2007 challenge achieved a mean H_d, Precession, Accuracy and MER of 5.48, 0.9698, 0.9812, and 0.7273, respectively. The results shown in Table 2, additionally tested by intra-region (I_h) uniformity, well known Pratt's Figure of Merit (FOM), reflect the credibility of DroLoG. Although the method is tested on all training datastes of MICCAI and [18], only the average values of a few subjects are shown in the Table.

In this paper, we present a modified graph-based approach that first enhances the image, utilizing noise. The enhancement module has shown promising results for subsequent use in graph-based segmentation. DroLoG has been shown as a desirable weighting function for the graph-based approach, compared with Gaussian or DoG. Interestingly, the proposed method performs quite well on all subjects of both imaging modalities. In future, we plan to extend this method to other imaging modalities.

Table 2: Segmentation evaluation.

Sub	Method	I_h	FOM	H_d	Prec.	Acc.	MER
# 1	*Gaussian*	3.81	0.68	5.98	0.8297	0.8291	0.9887
	DroLoG	3.48	0.83	5.16	0.9793	0.9896	0.7099
# 4	*Gaussian*	5.56	0.68	6.35	0.8206	0.8211	0.9943
	DroLoG	5.22	0.81	5.65	0.9679	0.9674	0.7932
# 7	*Gaussian*	5.24	0.68	6.28	0.8321	0.8310	0.9891
	DroLoG	5.14	0.84	5.60	0.9829	0.9969	0.7127
# 11	*Gaussian*	4.03	0.67	6.07	0.8267	0.8278	0.9912
	DroLoG	3.46	0.82	5.23	0.9839	0.9861	0.7020
# 14	*Gaussian*	4.34	0.64	6.25	0.8345	0.8336	0.9825
	DroLoG	4.04	0.91	5.06	0.9733	0.9988	0.7210
# 17	*Gaussian*	4.60	0.77	6.32	0.8326	0.8319	0.9856
	DroLoG	4.02	0.84	5.61	0.9724	0.9988	0.7231
# 22	*Gaussian*	4.69	0.76	6.38	0.8299	0.8298	0.9872
	DroLoG	4.13	0.83	5.40	0.9791	0.9897	0.7100

4. REFERENCES

[1] Frangi A.F., Niessen W.J., and Viergever M.A., "Three-dimensional modeling for functional analysis of cardiac images, a review," IEEE TMI, vol. 20, pp. 2−5, 2001.

[2] Dakua S.P. and Sahambi J.S., "Automatic LV contour extraction from CMR images using CB and random walk approach," Cardiovascular Engineering, Springer, vol. 10, pp. 30−43, 2009.

[3] Li C., Xu C., Gui C., and Fox M., "Level set formulation without re-initialization: a new variational formulation," In: IEEE CVPR, Vol. 1, pp. 430−436, 2005.

[4] Paragios N., "A level set approach for shape-driven segmentation and tracking of the left ventricle," IEEE TMI, vol. 22, pp. 773−776, 2003.

[5] Adalsteinsson D. and Sethian J., "A fast level set method for propagating interfaces," Journal of Computational Physics, vol. 118, pp. 169−277, 1995.

[6] Gonzalez R., Deschamps T., Idica R., Malladi R., and Solorzano C., "Automatic segmentation of histological structures in mammary gland tissue sections," Lawrence Berkeley National Laboratory, pp. 1−29, 2004.

[7] Chan T. and Vese, L., "Active contours without edges," IEEE TIP, vol. 10, pp. 266−277, 2001.

Table 1: The employed metrics for quantitative evaluation.

Measure	Definition
Hausdorff distance (HD)	Minimum distance between two sets of points
intra-region (I_h)	Index of homogeneity
Figure of Merit (FOM)	Segmentation index of matching with ground truth equivalent
Precision	True positive/(True positive + false positive)
Accuracy	(True positive + true negative)/total samples
Mean error rate (MER)	(False positive + false negative)/total samples × 100

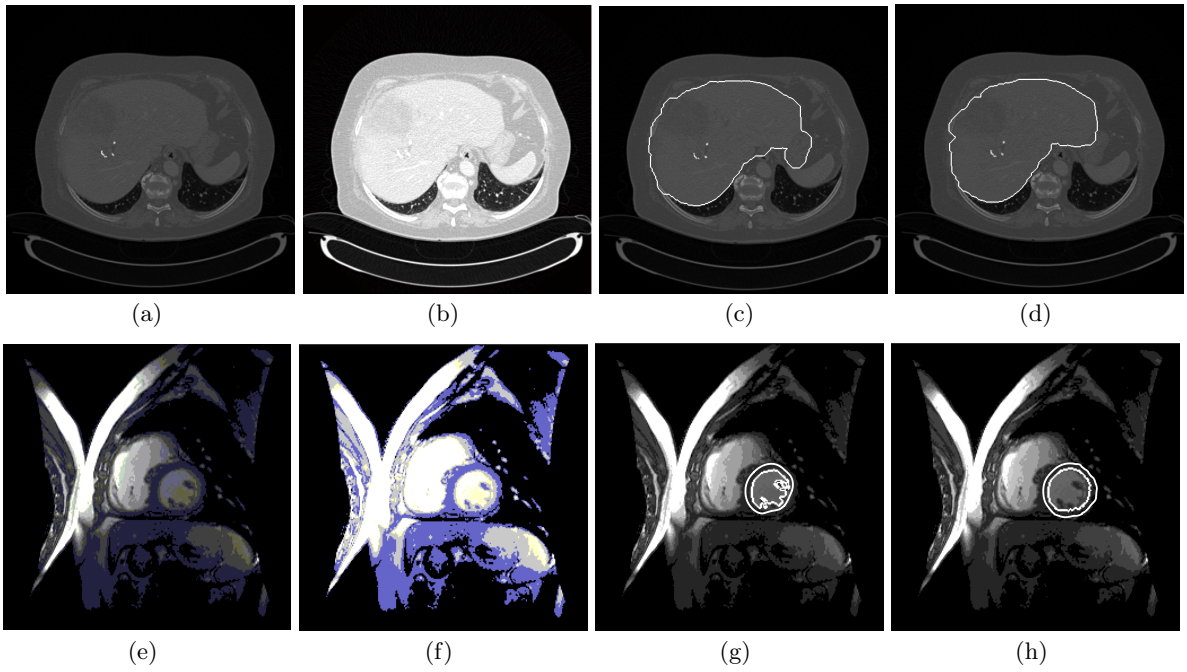

Figure 2: (a,e) Input CT and MR image. (b,f) Contrast enhancement at iteration count 300. (c,g) Segmentation due to Gaussian and (d,h) DroLoG.

[8] Davatzikos C., Vaillant M., Resnick S., Prince J., Letovsky S., and Bryan R., "A computerized method for morphological analysis of the corpus callosum," J. Comp. Assist. Tom, vol. 20, pp. 88−97, 1996.

[9] Cuadraa M., Craeneb M., Duaya V., Macqb B., Polloac C., and Thirana J., "Dense deformation field estimation for atlas-based segmentation of pathological MR brain images," Comput. Meth. Prog. Biomed., vol. 84, pp. 66−75, 2006.

[10] Vincent L. and Soille P., "Watersheds in digital spaces: An efficient algorithm based on immersion simulation," IEEE TPAMI, vol. 13, pp. 583-598, 1991.

[11] Sijbers J., Scheunders P., Verhoye M., Linden A. and Dyck, D., "Watershed-based segmentation of 3D MR data for volume quantization," Magnetic Resonance Imaging, vol. 15, pp. 679-688, 1997.

[12] Qazi A., Kim J., Pekar V., "Probabilistic refinement of model-based segmentation: application to radiation therapy planning of the head and neck," In Medical imaging and augmented reality, vol. 6326 of LNCS., Springer, pp. 403−410, 2010.

[13] Rallabandi V. and Roy P., "MRI enhancement using stochastic resonance in Fourier domain", MRI, vol. 28, pp. 1361-1373, 2010.

[14] Gard T., "Introduction to stochastic differential equations", New York: Marcel-Dekker, 1998.

[15] Grady L., "Random walks for image segmentation," IEEE PAMI, vol. 28, pp. 1-17, 2006.

[16] Jianbo S. and Malik J., "Normalized cuts and image segmentation," IEEE PAMI, vol. 22, pp. 888−905, 2000.

[17] Dakua S. and Sahambi J., "Modified active contour model and Random Walk approach for left ventricle CMR image segmentation," IJNMBE, Wiley, vol. 27, pp. 1350-1361, 2011.

[18] Andreopoulos A. and Tsotsos J., "Efficient and generalizable statistical models of shape and appearance for analysis of cardiac MRI," Medical Image Analysis, vol. 12, pp. 335-357, 2008.